Simulation-based Evaluation of NEG-ML Iterative Reconstruction of low count PET data

Louise Grèzes-Besset, Johan Nuyts, Ronald Boellard, Irène Buvat, Christian Michel, Christian Pierre, Nicolas Costes, Anthonin Reilhac

***Abstract*—In this study we propose the use of a new reconstruction scheme for low count data which consists in the reconstruction of the prompt events with the inclusion of the correction of the sources of contamination in the iteration process (OP-scheme) using the NEG-ML algorithm. The performances of this variant, hereafter called OP-NEG3D, is evaluated in low count data situations using simulated replicated data. Quantification results obtained with the filtered back projection algorithm (FBP3D), which is still the standard reconstruction method for quantitative dynamic PET brain studies, and conventional OP-OSEM3D are also shown for comparisons. The comparison tests include the VOI-based measurements of activity concentrations in large regions filled with high and low activity concentrations, the measurement of small activity differences in hot and cold regions using VOIs and using voxel-wise statistical analysis, and the activity recovery in small cold and hot inserts. The results indicated that OP-NEG3D allows an activity recovery in large cold regions as accurate as with FBP3D whereas OP-OSEM3D is biased due to the positivity constraint in the image space. OP-NEG3D shows better noise characteristics than FBP3D and allows a better detectability of differences between groups of scans and a better recovery of the activity in small regions than FBP3D. In conclusion, OP-NEG3D is a viable alternative to FBP3D for the reconstruction of PET data in the context of dynamic brain imaging.**

I. Introduction

STATISTICAL image reconstruction methods such as MLEM [1] have shown improved image quality over conventional analytical reconstruction methods. Indeed, they account for the noise nature, and may include in the iteration process the correction for the image degrading factors such as attenuation, normalization, scattered and random events contamination and finite spatial resolution. Therefore, they yield images with a lower variance, an enhanced contrast and resolution and a better signal-to-noise ratio compared to images reconstructed with an analytical method [2]–[7]. In the case of sinograms containing few events, as in dynamic radio-ligand PET studies where early frames are usually short in time and where the radio-activity is low for the late frames due to activity decay, the activity estimate obtained with ML-based reconstruction methods is biased by the built-in positivity constraints in the sinogram space and in the image space. Both constraints contribute to an overestimation of the activity in cold regions of the image [8]. First, the reconstruction of the pre-corrected sinograms raises two issues. Pre-corrected data result from the subtraction of the estimated scatter distribution and the estimated or measured random distribution from the detected prompt events. In addition to affecting the Poisson nature of the detected prompt events, this operation yields negative elements in the sinogram [9]. Those negative elements are set to zero prior to the reconstruction which results in locally overestimated counts (higher counts are no longer counter balanced by negative counts). The reconstruction of the prompt events, called Ordinary Poisson OSEM (OP-OSEM [9]), with the inclusion of the correction of the sources of contamination in the iteration process offers a valuable solution to these issues. Second, the MLEM algorithm can be regarded as a scaled gradient ascent algorithm, in which the step size is such that it prevents negative values:

$$\lambda_j = \lambda'_j + \Delta_j \sum_i c_{ij} \frac{y_i - r'_i}{r'_i} \tag{1}$$

where prime indicates the reconstruction available at the current iteration, y_i is the measured count in detector i, λ_j is the unknown activity in pixel j, c_{ij} is the system matrix, r_i is the projection estimate $r_i = \sum_j c_{ij}\lambda_j$ and Δ_j is the step size. With the conventional MLEM algorithm the step size is given by:

$$\Delta_j = \frac{\lambda'_j}{\sum_i c_{ij}} \tag{2}$$

The main disadvantage of this step size calculation is that it vanishes when λ'_j approaches zero. In other words, for activities near zero, the step size can be very small leading to very slow (or unreachable) convergence. This is especially true when the data to be reconstructed are noisy and contain few events. The *premature* interruption of the iteration process is the second source of the activity overestimation in *cold regions*. Methods such as AB-EMML [10] and NEG-ML [11] are alternatives to MLEM which allow negative values in the image and a faster convergence to low activity values. These methods should help in decreasing the bias of cold regions. The NEG-ML algorithm, developed in the context of whole-body reconstruction of PET data without attenuation correction, followed an approach similar to the surrogate function method proposed by Ahn and Fessler [12]. In NEG-

Louise Grèzes-Besset, Christian Pierre, Nicolas Costes and Anthonin Reilhac are with the CERMEP, 59 boulevard Pinel, F-69667 Bron, France.(e-mail: anthonin.reilhac@cermep.fr)

Johan Nuyts is with the Katholiek Universiteit Leuven, U.Z. Gasthuisberg, Herestraat 49 B3000, Leven, Belgium.

Ronald Boallaard is with the clinical PET Center, University Hospital Vrije Universiteit, Amsterdam, The Nethrelands

Irène Buvat is with U678 Inserm, CHU Pitié Salpêtrière, Paris, France

Christian Michel is with Siemens Medical Solutions, Molecular Imaging, Knoxville, TN, 37932, USA

1-4244-0923-3/07/$25.00 ©2007 IEEE.

ML, an alternative step size is derived as follows:

$$\Delta_j = \frac{1}{\sum_i \frac{c_{ij}}{y_i} \sum_\xi c_{i\xi}} \tag{3}$$

where ξ is the image pixel index equivalent to j. Unlike the MLEM step size, this step size does not vanish when the pixel value gets close to zero. To avoid zero divisions in the above equation and in the ML equation, $\frac{1}{y_i}$ or $\frac{1}{r'_i}$ are replaced by 1 whenever y_i or r'_i is smaller than 1. This step size can be very small for positive pixel values. To improve the convergence speed, the MLEM step size is also computed in every pixel and the algorithm uses the largest of the MLEM and NEG-ML step sizes.

$$\Delta_j = max \left[\underbrace{\frac{\lambda'_j}{\sum_i c_{ij}}}_{\text{MLEM}}, \underbrace{\frac{1}{\sum_i \frac{c_{ij}}{y_i} \sum_\xi c_{i\xi}}}_{\text{NEG-ML}} \right] \tag{4}$$

In this study we propose the use of a new reconstruction scheme for low count data which consists in the reconstruction of the prompt events with the inclusion of the correction of the sources of contamination in the iteration process (OP-scheme) using the NEG-ML algorithm. The performances of this variant, hereafter called OP-NEG3D, is evaluated in low count data situations using simulated replicated data. Quantification results obtained with the filtered back projection algorithm (FBP3D), which is still the standard reconstruction method for quantitative dynamic PET brain studies, and conventional OP-OSEM3D are also shown for comparisons. A special focus is put on the evaluation of the performances of the reconstruction methods for the quantification of low activities and for the quantification of small activity differrences using simulated cases.

II. Material and Methods

A. Absolute activity and relative difference as a function of the count level

1) Data simulation: Several simulated replicated data were generated for 4 different count levels characterized by the NEC (Noise Equivalent Count): NEC = 47.85 k counts (extremely low), 1.44 M counts, 3.35 M counts and 16.7 M counts (regular count level), using the PET-SORTEO Monte Carlo PET simulator [13], [14], modeling the Ecat Exact HR+ scanner operating in 3D mode. The phantom used for the simulation consisted of 3 cylindrical compartments filled with radioactive fluorine: the main compartment, denoted hereafter by *Background* (Φ = 20 cm, length = 20 cm) and 2 cylindrical inserts denoted hereafter by *hot region* (Φ = 5 cm, length = 20 cm), and by *cold region* (Φ = 9 cm, length = 20 cm). For all count levels but the highest, 50 equivalent replicates (hereafter called group 1) were simulated from the phantom filled with a homogeneous activity of 100 Bq/cc in the background, 10 Bq/cc in the cold region and 300 Bq/cc in the hot region. For the highest count level only 10 replicated data were generated. The chosen attenuation phantom, activity level, detection geometry and acquisition parameters lead to an average scatter fraction of 43.25% and an average random fraction of 18%. For each of the 4 count levels (or NEC), other equivalent replicates (group 2) were simulated following the same methodology as for the creation of group 1, but with the activities in the inserts increased by 5%.

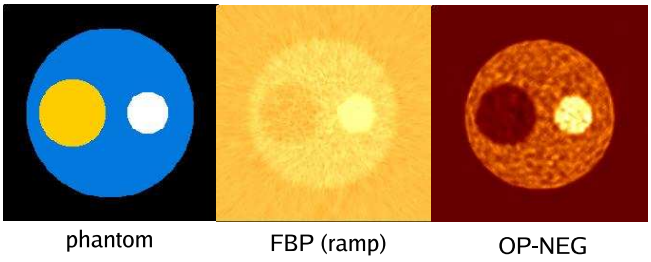

Figure 1. (left) original numerical phantom employed for the simulation. (middle) the FBP3D image and (right) the OP-NEG3D images reconstructed from a single replicate (NEC = 3.35 M counts).

2) Data correction and reconstruction: Two iterative reconstruction variants were tested: 1) Ordinary Poisson (OP) using the conventional MLEM algorithm (OSEM implementation), hereafter called OP-OSEM3D and 2) OP using the NEG-ML flavour, hereafter called OP-NEG3D. In the OP-variants, the volume is directly reconstructed from the prompt events with the estimated random event and scatter event distributions as sources of contamination. For this, a mean (and smooth) random event distribution was derived, for each simulated group, from the simulation of 120,000 independent realizations of random events. A random estimate was then derived for the correction of each count level by appropriately scaling down the original distribution. A smooth scattered event distribution was estimated using the e7_sino program (e7tools package) from the sum of the replicates with the highest NEC. The scatter distribution was then globally scaled down to derive a scatter distribution estimate matching each count level. We followed this strategy to avoid including bias and variability from the scatter and random correction procedure in the comparison of the algorithm performances. Data were also reconstructed using a filtered back projection algorithm (FBP3D), using a ramp filter and a cut-off frequency of 0.5 cm^{-1}. We used the scatter distribution estimate for the pre-correction of the scatter with FBP3D. Each reconstruction led to 63 axial slices of 128x128 voxels (2.25 x 2.25 x 2.4250 mm^3). Figure 1 shows the original numerical phantom employed for the simulation, the FBP3D image and the OP-NEG3D image reconstructed from a single replicate (NEC = 3.35 M counts). Preliminary results showed that the number of iterations required to ensure convergence in the cold region (the slowest to converge) were different depending on the count level, and also on the reconstruction variant. Table I shows the number of iterations and subsets required to reach convergence with all reconstruction methods and for each count level.

3) Analysis:

- Using the available reconstructed data from group 1 at each count level, mean activity, mean coefficient of variation of the measurement (COV), and standard deviation

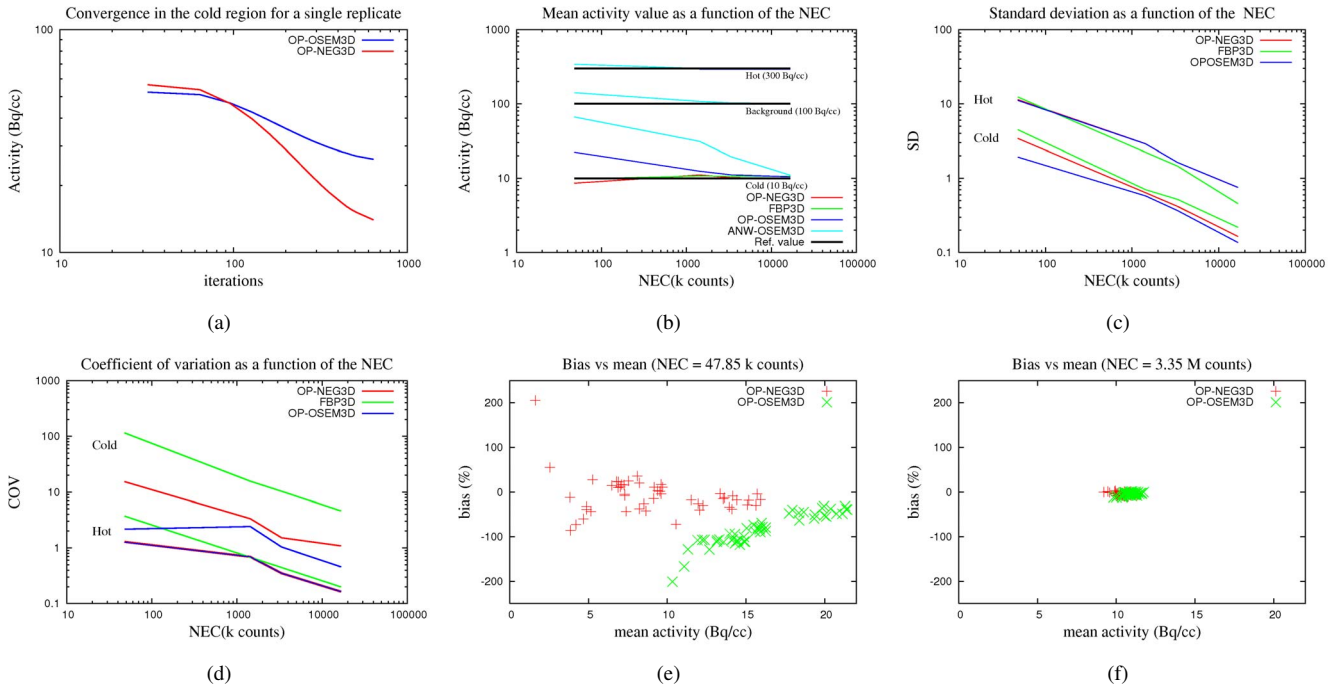

Figure 2. (a) Activity values measured in the cold region as a function of the number of iterations. (b) Mean activity measured in the 3 compartments as a function of the NEC. (c) Standard deviation of the measurements as a function of the NEC. (d) Coefficient of variation of the measurement as a function of the NEC. (e-f) scatter plots of the relative differences between the cold region activity values measured from the reconstructed FBP3D images and from the OP-NEG3D and OP-OSEM3D images as a function of the mean activity values computed from the 50 replicates and for two NEC levels.

Table I
NUMBER OF ITERATIONS AND SUBSETS USED FOR EACH COUNT LEVEL

NEC (counts)	Iterations x Subsets	MLEM equivalent iteration
47.85 k	13x32 + 8x16 + 8x8 + 8x4	640
1.44 M	3x32 + 8x16 + 8x8 + 8x4	320
3.35 M	3x32 + 4x16 + 4x8 + 8x8	224
16.7 M	3x32 + 4x16 + 4x8 + 8x8	224

(SD) were calculated in Volumes of Interest (VOIs) The VOIs were slightly smaller than the actual regions so as to prevent bias due to activity contamination from the other regions. The COV was computed as the ratio of the standard deviation of the values of the pixel belonging to VOI to the mean pixel value in the VOI. The mean COV was the average COV calculated for each replicated data, and it reflected the homogeneity of the pixel values within the VOI. The SD characterized the dispersion of the mean VOI values computed from all replicated data from a specific NEC level.

- We characterized the activity differences in the hot and cold regions between the two groups of scans as a function of the NEC, by computing the VOI-based mean activity differences. The signal to noise ratio (SNR), computed as the ratio of the mean activity difference measured from the replicated data to the standard deviation was also derived.
- Finally, the detectability of the differences between the two groups of scans was characterized voxel-wise for the NEC level of 3.35 M counts using a 2 sample t-test with SPM2 (Statistical Parametric Mapping, Welcome Department of Cognitive Neurology, London), as a function of the number of scans included in the analysis. The sensitivity was computed as the ratio of the detected true positive voxels to the total number of voxels which should be detected as significantly different. As in actual SPM analysis, spatial smoothing was applied to the data prior to the analysis. We tested Gaussian smoothing of 4, 8, 12 and 16 mm full width half maximum (FWHM). The mean Z-score was also determined.

B. *Activity recovery in small regions*

1) Data simulation: Following the same methodology as in the previous section we generated several replicated data for different NEC values (ranging from 47.85 k counts to 16.7 M counts). The employed phantom consisted in a main cylindrical compartment (Φ = 20 cm, length = 20 cm) with small line inserts with diameters of 5, 8, 10 and 12 mm. Half of the inserts were filled with a homogeneous activity of 10 Bq/cc and the others were filled with a homogeneous activity of 300 Bq/cc while the activity in the main compartment was held at 100 Bq/cc. A total of 480 equivalent MLEM iterations were used for the iterative reconstruction (11 x 32 + 4 x 16 + 8 x 8 [iteration x subset]) using OP-OSEM3D and OP-NEG3D using scatter and random contamination estimates derived as in the previous section. The selected number of iterations was selected as a compromise between the numbers of iterations required for convergence in case of low and high count cases, and was not optimized for each NEC level. In order to assess the impact of the number of iterations on the activity recovery in small regions, data were also reconstructed with OP-NEG3D using 640 equivalent MLEM iterations (13x32 +

8x16 + 8x8 + 8x4 [iteration x subset]). The data were also reconstructed using FBP3D, using a ramp filter and a cut-off frequency of 0.5 cm^{-1}. Each reconstruction led to 63 axial slices of 128x128 voxels (2.25 x 2.25 x 2.4250 mm^3).

2) Analysis: For each count level, the mean activity in each insert was extracted using VOIs from each of the reconstructed replicated scans and averaged. A global activity value was derived for the hot and the cold inserts by averaging the activity values obtained for each insert diameter.

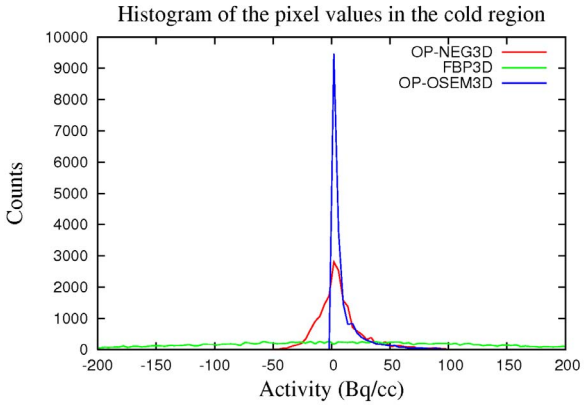

(a) NEC = 1.44 M counts

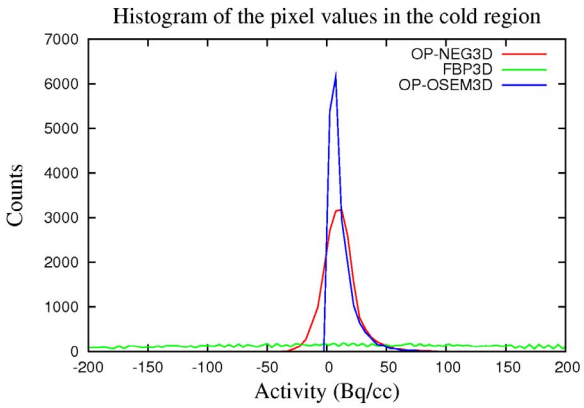

(b) NEC = 3.35 M counts

Figure 3. Histograms of the pixel values in the cold region from a single replicate reconstructed with OP-NEG3D, OP-OSEM3D and FBP3D and for two count levels: (a) NEC = 1.44 M counts and (b) NEC = 3.35 M counts.

III. Results

Images reconstructed with FBP3D and OP-NEG3D and from a single replicate scan (NEC = 3.35 M counts) are shown in figure 1. The OP-OSEM3D image is very similar to the OP-NEG3D image. Generally speaking, iterative reconstruction methods led to images with higher visual image quality. Figure 2(a) shows the activity measured in the cold region as a function of the number of iterations used for the reconstruction and from images reconstructed with OP-NEG3D and OP-OSEM3D operating on a single scan from the group with the lowest NEC. This result is representative of the convergence characteristics. This figure demonstrates that the convergence is faster with OP-NEG3D than with OP-OSEM3D in the cold region. The slower convergence to low

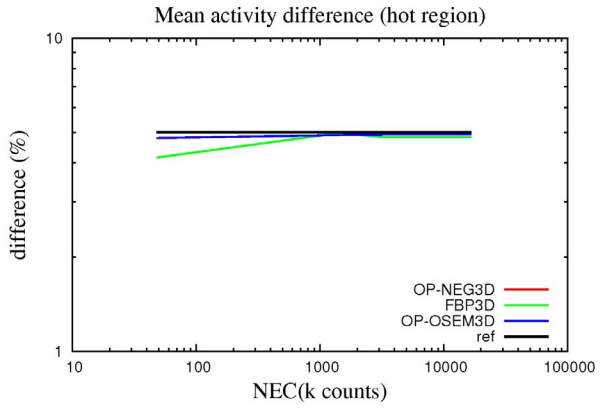

(a)

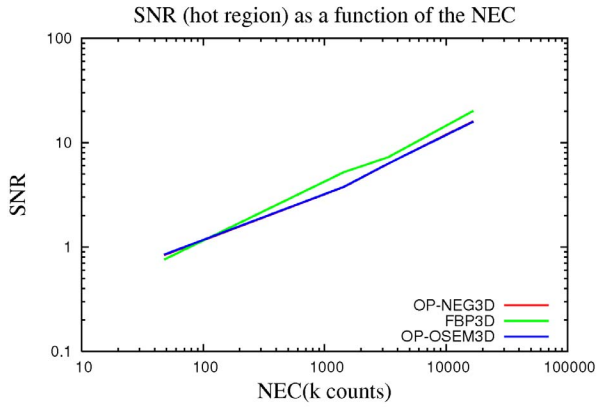

(b)

Figure 4. (a) Mean activity differences (%) and (b) SNR measured in the hot region between replicated data from group 1 and group 2 at various NEC levels. The reference difference in the hot region is 5%

activity values of OP-OSEM3D leads to an overestimation of the *cold region* activities as compared to the values obtained with OP-NEG3D when the count level is low. This is also visible in figure 2(b), which represents the estimated mean activity values computed from all replicates as a function of the NEC and for the different reconstruction methods. Mean activity values obtained with ANW-OSEM3D (Attenuation and Normalization Weighted- OSEM) and FBP3D are also reported for comparison. In addition to being biased by the positivity constraint in image space, ANW-OSEM3D reconstruction also suffers from the positivity constraint in sinogram space since data are pre-corrected for the scatter and random contaminations with this reconstruction variant. While OP-OSEM3D significantly reduced the positive bias in the cold region as compared to ANW-OSEM3D reconstructions, only OP-NEG3D was able to completly remove it. Figure 2(c) shows the standard deviation of the activity measurements in the hot and cold regions computed for each NEC level using the 50 replicated data sets. It shows that in low activity situations, iterative reconstruction methods outperform FBP3D (see the cold region), OP-OSEM3D being the best method regarding this criterion. In higher activity situations, FBP3D seems to perform slightly better than OP-NEG3D and OP-OSEM3D whose curves are almost superimposable. It could be

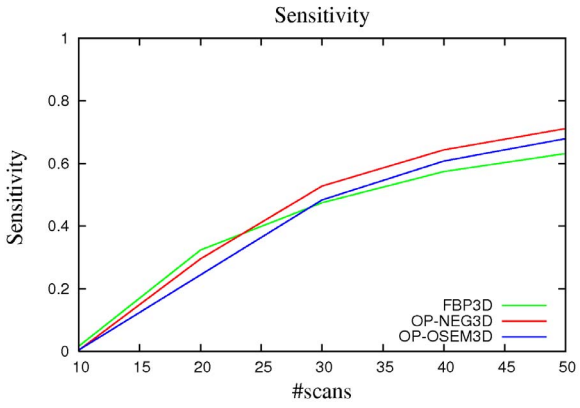

(a) FWHM = 12 mm

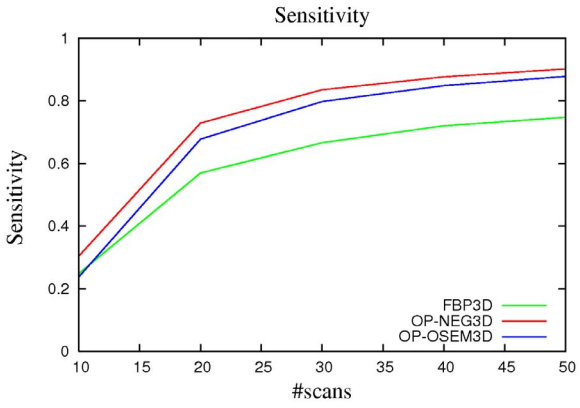

(b) FWHM = 16 mm

Figure 5. Sensitivy obtained from a voxel-wise two sample t-test with SPM2 as a function of the number of reconstructed volumes per group involved in the analysis. Volumes were reconstructed using OP-NEG3D, OP-OSEM3D and FBP3D.

that the selected number of iterations was not optimal in these cases. Figure 2(d) shows the measured COV in the images. The results suggest that iterative reconstruction methods produce images with a lower noise than FBP3D, whatever the region and the count level. This is an important advantage of iterative methods over FBP3D. Figures 2(e) and 2(f) are the scatter plots computed from the 50 replicates and for two NEC levels of the relative differences between the cold region activity values measured from the FBP3D images and from the OP-NEG3D (respectively OP-OSEM3D) images as a function of the mean activity values measured from the FBP3D images and from the OP-NEG3D (respectively OP-OSEM3D) images. The results shows that a low count level there are large relative differences between the cold region activity values measured from the FBP3D and OP-OSEM3D reconstructed volumes. The differences are less important at higher count level. Differences between the cold region activity values measured from the FBP3D and OP-NEG3D are less important whatever the count level.

The histograms of the pixel values in the cold region from a single replicate reconstructed with OP-NEG3D, OP-OSEM3D and FBP3D are shown for two NEC levels in figure 3. The histograms clearly show the truncation of the pixel value distributions for negative values with OP-OSEM3D reconstruction which leads to an overestimation of the activity. The pixel value distribution obtained with OP-NEG3D is not truncated, almost symmetric and centered on the true activity value. FBP3D also led to symetric pixel value distributions centered on the exact value. However, the dispersion of the pixel counts was much larger than with OP-NEG3D.

Figure 4(a) shows the mean percent differences between the activity values measured between replicated data from the two groups of scans at various NEC levels. The true activity difference in the simulated data was 5%. The results show that all methods were able to accurately estimate the difference at all NEC except at the lowest iterative methods outperformed FBP3D. OP-NEG3D and OP-OSEM3D performed similarly and their respective curve are almost superimposable. It must be noted that none of the tested methods was able to characterize the 5% difference in the cold region between the two groups of scans. The signal to noise ratio of the difference measurements obtained with the studied reconstruction methods is shown in figure 4(b) as a function of the NEC. The results show that FBP3D very slightly outperformed iterative reconstruction methods at all NEC levels but the lowest.

Figure 5 shows difference detectability results obtained with a 2 sample t-test with SPM2 and for the NEC level of 3.35 M counts. The graph gives the obtained sensitivity for each reconstruction method and for two smoothing parameters as a function of the number of scans involved in the statistical analysis. The results indicate that at a smoothing of 12 mm, OP-NEG3D is the reconstruction enabling the highest sensitivity when the number of scans is greater than 25, while with less than 25 scans, FBP3D is slightly more sensitive. The results obtained with a higher smoothing are clearly at the advantage of iterative reconstruction methods and especially OP-NEG3D. From these results it seems that the same smoothing process increases the sensitivity more when applied to iteratively reconstructed PET data than on FBP3D reconstructed data. The lower COV of OP-NEG3D and OP-OSEM3D images might be at the origin of this finding. No voxels were found significantly different with a Gaussian smoothing of 4 mm for any method, and a smoothing of 8 mm showed a slight superiority of FBP3D over iterative reconstruction methods. The mean Z-score obtained with FBP was very slightly better than with iterative reconstruction methods.

Figure 6 shows the activity recovery in the hot and cold regions, obtained with the studied reconstruction methods as a function of the NEC. Since we used the same number of iterations (480 and 640 for OP-NEG3D and 480 for OP-OSEM3D) for all NEC levels, the performance obtained with iterative reconstruction methods strongly depends on the count level. Indeed, the higher the count level, the better the recovery. The results show that iterative reconstruction methods outperform FBP3D for NEC values above 200 k counts in the hot region and above 800 k counts in the cold region, with, in both cases, a slight advantage of OP-NEG3D over OP-OSEM3D. The higher performances of iterative reconstruction methods over FBP3D are mainly due to the spatial degradation modeling in the iteration loop. The better performances offered by OP-NEG3D over OP-OSEM3D are almost certainly due to its

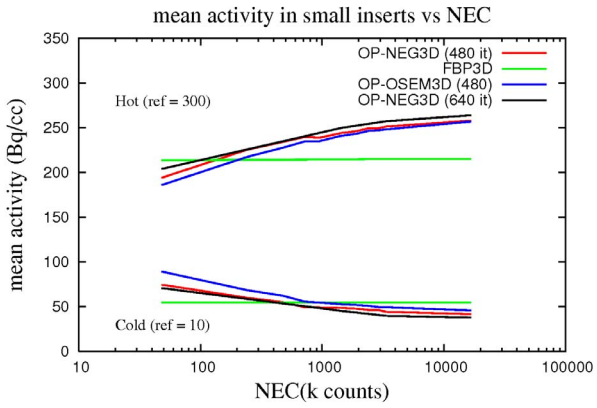

Figure 6. Activity recovery in the small hot and cold inserts obtained with OP-NEG3D, OP-OSEM3D anf FBP3D reconstruction method as a function of the NEC.

faster convergence. A higher number of iterations improves the performances of the iterative reconstruction methods (see the results obtained with OP-NEG3D using 480 and 640 equivalent ML-EM iterations).

IV. Conclusion

In this study we investigated and compared the performances of three reconstruction methods, OP-NEG3D, OP-OSEM3D and FBP3D in the case of the reconstruction of low count PET data. The comparison tests included the VOI-based measurements of activity concentrations in large hot and cold regions, the measurements of small activity differences in hot and cold regions using VOI and using voxel-wise statistical analysis, and the activity recovery in small cold and hot inserts. The results indicated that OP-NEG3D allows an activity recovery in large cold regions as accurate as with FBP3D whereas OP-OSEM3D is biased due to the positivity constraint in the image space. OP-NEG3D shows better noise characteristics than FBP3D and allows a better detectability of differences between groups of scans and a better recovery of the activity in small regions than FBP3D. While OP-NEG3D seems to be an interesting alternative to FBP3D for the reconstruction of dynamic brain PET data where the count levels in each frame are generally low, the actual gain remains to be assessed in more realistic conditions. We plan to assess the performance of the reconstruction algorithm on simulated data of dynamic radio-ligand PET acquisitions as was already performed in [8] for ANW-OSEM3D and UW-OSEM3D (UnWeighted-OSEM).

References

[1] L. A. Shepp and Y. Vardi, "Maximum likelihood reconstruction in positron emission tomography,," *IEEE Trans. Med. Imaging*, vol. 1, no. 2, pp. 113–122, 1982.

[2] Y. Bouchareb, K. Thielemans, T. Spinks, O. Rimoldi, and P. G. Camici, "Comparison of analytic and iterative reconstruction methods for quantitative cardiac PET studies in 3D using Oxygen-15 water scans," in *IEEE Nuclear Science Symposium Conference Record*, vol. 4, pp. 2120–2123, 2005.

[3] C. Riddell, R. E. Carson, J. A. Carrasquillo, S. K. Libutti, D. N. Danforth, M. Whatley, and S. L. Bacharach, "Noise reduction in oncology FDG PET images by iterative reconstruction: a quantitative assessment," *J. Nucl. Med.*, vol. 42, pp. 1316–23, Sept. 2001.

[4] F. Gutman, I. Gardin, N. Delahaye, H. Rakotonirina, A. Hitzel, A. Manrique, D. L. Guludec, and P. Véra, "Optimisation of the OS-EM algorithm and comparison with FBP for image reconstruction on a dual-head camera: a phantom and a clinical 18F-FDG study," *Eur. J. Nucl. Med. Mol. Imaging*, vol. 30, pp. 1510–9, Nov. 2003.

[5] C. X. Wang, W. E. Snyder, G. Bilbro, and P. Santago, "Performance evaluation of filtered backprojection reconstruction and iterative reconstruction methods for PET images," *Comput. Biol. Med.*, vol. 28, pp. 13–24, Jan. 1998.

[6] R. Boellaard, A. van Lingen, and A. A. Lammertsma, "Experimental and clinical evaluation of iterative reconstruction (OSEM) in dynamic PET: quantitative characteristics and effects on kinetic modeling," *J. Nucl. Med.*, vol. 42, pp. 808–17, May 2001.

[7] J. Nuyts and J. A. Fessler, "A penalized-likelihood image reconstruction method for emission tomography, compared to postsmoothed maximum-likelihood with matched spatial resolution.," *IEEE Trans. Med. Imaging*, vol. 22, pp. 1042–52, Sept. 2003.

[8] A. Reilhac, S. Tomeï, I. Buvat, C. Michel, F. Keheren, and N. Costes, "Simulation-based evaluation of OSEM iterative reconstruction methods in dynamic brain PET studies," *Neuroimage, in press*, 2008.

[9] M. Yavuz and J. A. Fessler, "Objective functions for tomographic reconstruction for random-precorrected PET scans," in *IEEE Nuclear Science Symposium Conference Record*, vol. 2, pp. 1067–1071, 1996.

[10] K. Erlandsson, D. Visvikis, I. C. W. A. Waddington, P. H. Jarrit, and L. S. Pilowsky, "Low-statistics reconstruction with AB-EMML," in *IEEE Nuclear Science Symposium Conference Record*, vol. 3, pp. 15/249–15/253, Oct. 2000.

[11] J. Nuyts, S. Stroobants, P. Dupont, S. Vleugels, P. Flamen, and L. Mortelmans, "Reducing loss of image quality because of the attenuation artifact in uncorrected PET whole-body images," *J. Nucl. Med.*, vol. 43, pp. 1054–62, Aug. 2002.

[12] S. Ahn and J. A. Fessler, "Emission image reconstruction for randoms-precorrected PET allowing negative sinogram values.," *IEEE Trans. Med. Imaging*, vol. 23, pp. 591–601, May 2004.

[13] A. Reilhac, G. Batan, C. Michel, C. Grova, J. Tohka, N. Costes, and A. C. Evans, "PET-SORTEO: Validation and development of database of simulated PET volumes," *IEEE Trans. Nucl. Sci.*, vol. 52, pp. 1321–1328, Oct. 2005.

[14] SORTEO, "http://sorteo.cermep.fr."